Naturally Occurring and Biomimetic Synthesized Calcite Spherulites

Shitao Wu,[†] Justine I. Blake,[†] Li Guo[‡] and Wuzong Zhou[†,*]

[†] EaStCHEM, School of Chemistry, University of St Andrews, St Andrews, Fife KY16 9ST, United Kingdom.

[‡] CASP, West Building, Madingley Rise, Madingley Road, Cambridge CB3 0UD, United Kingdom.

ABSTRACT: Naturally occurring calcite spherulitic particles were collected from East Kirkton Quarry in Bathgate, Scotland. Their microstructure has been revealed, by using XRD, EDX, SEM and HRTEM, to consist of a low crystallinity core with deposition of multilayer radially oriented calcite microrods. The surrounding materials of the spherulites are mainly Ca-free silicates. To understand the formation mechanism of this construction of calcite crystals, biomimetic synthesis of similar spherulites have been carried out by using alginate and stevensite as structure directing agents. It is found that alginate is essential for growth of the spherulites, since the spherulites are developed only when they are embedded in the alginate network, a soft matter substrate. Stevensite also plays an important role of adjusting the hardness of the alginate substrate, offering a suitable network for the self-aggregation and self-orientation of the calcite nanocrystals. Possible inter-particle interactions or driving force of the particle aggregation and self-orientation are discussed.

1. INTRODUCTION

Calcium carbonate has its own significance in biomineralization process. Spherulite is probably one of the most interesting morphologies of $CaCO_3$ found in natural creatures or biominerals, due to their complex constructions of inorganic and biological components and their radial arrangement of microrods.[1,2] Spherulites have also attracted increasing attention from geologists,[3-5] because carbonate spherulitic facies have been discovered to be excellent reservoirs from Early Cretaceous pre-salt oil fields in the South Atlantic.[6] However, the origin of the spherulites is uncertain.

Abundant carbonate spherulites occur in the Early Carboniferous alkaline lacustrine succession at East Kirkton, Scotland. This succession was formed in a rift setting and involved with volcanic activity.[7] It shows similarities with pre-salt spherulitic deposits in the South Atlantic.[8] For geologists, studying the formation mechanism of spherulitic $CaCO_3$ in this area helps the understanding of origin and development of pre-salt spherulites.

For material scientists, the spherulite with radially oriented microrods is an uncommon crystal morphology, which is not energy-minimized for any polymorphs of calcium carbonate. Due to very complicated chemical compositions and polycrystalline structures, our knowledge of the formation mechanisms of these spherulites is still very limited, although many people have made great efforts in this field. One of the previously proposed formation mechanisms is based on Brownian motion, i.e. spherulites can form via aggregation of tiny nanocrystallites (<10 nm) in Brownian motion.[9] However, Brownian motion can only occur in a solution, which may not be the case for the growth of most $CaCO_3$ spherulites in natural environments. Furthermore, the detailed microstructures and complicated morphologies of spherulites cannot be explained simply using Brownian motion.

A phase field effect was believed to be a more convincing explanation of the spherulitic growth.[10] It was based on the “diffusional instabilities”. The model indicated a competition between the ordering effect of discrete local crystallographic symmetries and the randomization of the local crystallographic orientation with growth front nucleation. This mechanism is also for

growth of spherulites in solution and the resulted dendrite microstructures are quite different from the spherulites of calcium carbonate we studied in this project.

Another important phenomenon of crystal growth, which is relevant to the spherulite formation, is aggregation based. Recently, Banfield et al.[11] revealed a three-dimensional rotation of nanoparticles (2 to 3 nm in diameter) in their high resolution transmission electron microscopic (HRTEM) study of natural iron oxyhydroxide biomineralization products. Neighbouring nanoparticles could aggregate and rotate to adopt parallel orientations.

For the naturally occurring spherulitic carbonate, there is a debate on whether the formation of these spherulites happens via a biotic or an abiotic process. Proposals for abiotic mechanisms cited a catalyzing role for "co-occurring minerals" during $CaCO_3$ precipitation.[6] Tosca and Wright [12] suggested Mg-silicate clays (stevensite) function as the co-occurring minerals which lead the spheroidal crystal formation. Workers who advocate a biotic mechanism infer organic acid as the origin of spheroidal formation, where extracellular polymeric substances (EPS) helped as active catalysts in the precipitation.[13] Alginic acid (also called alginate, which is a polysaccharide distributed widely in the cell walls of brown algae) is believed to be a suitable EPS catalyst to synthesize spherulites, because it is a common polymer produced by marine and terrestrial bacteria and it has a capability to overcome the kinetic limiting barrier for less-favoured components.[14] The biotic process uses the presence of organic acids which catalyse the reaction of the $CaCO_3$. There are also many studies involving the role of bacteria in spherulite formation.[1]

Mercedes-Martin, et al.[15] tried to find the origin of spherulites by using stevensite and alginic acid in their synthetic systems, in order to clarify which substance was crucial to the formation of spherulites. They found that spherulites could form when alginate was present without stevensite. However, no gel formed in their synthetic systems. The detailed inner structures of the spherulites were not analyzed and the hollow spherical particles looked quite different from the commonly observed naturally occurring spherulites with radial arrangement of microrods.

In our previous biomimetic synthesis of calcium carbonate spherulites in presence of gelatin as a structure directing agent, we found the main component, needle-like microrods, is polycrystalline, containing nanocrystallites embedded in gelatin. The nanocrystallites can self-orientate driven by dipolar field interaction.[16] On the other hand, similar naturally occurring spherulites were previously found in a limpet shell where the particles were embedded in biological substance.[17] It seems to be true that gelatin has a similar function as alginate, both being negatively charged polymerized biological substances. It is of interest to establish the formation mechanism of calcium carbonate spherulites and to understand why a soft polymerized biological substance is essential for the growth of $CaCO_3$ spherulites.

In the present work, we have investigated the microstructures of the naturally occurring calcite spherulites and biomimetically synthesized similar spherulites in presence of alginate and/or stevensite. With better understanding of the structures, we are able to propose a formation mechanism of spherulites.

2. EXPERIMENTAL SECTION

Collection of natural samples. Spherulitic limestone samples were collected from East Kirkton quarry, Scotland, which consists of ac. 10 m thick dominated lacustrine carbonates deposited in a rift basin within a volcanic terrain during Early Carbon-iferous.[18] Spherulitic limestones occur as different sized layers alternating with bioclastic limestones, microbiallimestones and mudstones.

A typical spherulitic limestone sample chiselled from a 15-meter-thick limestone succession is shown in Figure 1. In some layers, as marked by the yellow arrows, many spherulites (1 to 2 mm in diameter) were recognized and collected for the present studies.

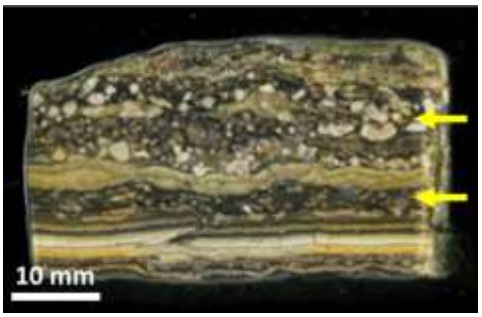

Figure 1. A typical rock sample collected from East Kirkton Quarry, Bathgate, Scotland. The layers marked by the yellow arrows contain many calcite spherulites.

Biomimetic synthesis of spherulites. Synthesis of $CaCO_3$ spherulites was carried out, using $CaCl_2$ and Na_2CO_3 as precursors, and sodium alginate and stevensite as structure directing agents. Nine different formula of synthetic systems were used as shown in Table 1, resulting in nine groups of products. In each group, several specimens were collected at different reaction times.

Table 1. Compositions of the synthetic systems for spherulites and main products containing bulk crystals (B) and/or spherulites (S).

Gr	$CaCl_2$ (mmol)	Na_2CO_3 (mmol)	Stevensite (mg)	Alginate (mg)	Main Prod.
1	5.0	5.0	0	0	B
2	5.0	5.0	10	0	B
3	5.0	5.0	0	10	B&S
4	5.0	5.0	10	10	B&S
5	5.0	5.0	100	100	B&S
6	5.0	5.0	0	1000	S
7	5.0	5.0	1000	1000	S
8	5.0	5.0	0	2000	S
9	5.0	5.0	2000	2000	S

$CaCl_2$ (>98.0%, Merck KGaA) and Na_2CO_3 (>99.0%, Sigma-Aldrich) were used as received without further purification. Sodium alginate was purchased from Sigma-Aldrich with the molecular weight ranging from 80,000 - 120,000. The polymeric structure of alginate contains repeating units of β-D-mannuronic acid and α-L-gluronic acid, respectively.[19]

The preparation of stevensite refers to Tosca and Wright [12] in order to simulate the surrounding substance of the spherulites in natural environment. The molar quantities (mmol) of the chemicals in the synthesis of stevensite are: 50.0 $Al(NO_3)_3$: 7.06 $NaNO_3$: 63.6 $Mg(NO_3)_2$: 3.52 $Ca(NO_3)_2$: 85.0 SiO_2 : 254 urea. Fumed silica was first added to 200 mL deionised water in a 500 mL flask and was heated under reflux for 1 h. The remaining salts were dissolved in water (50 mL), then added to the silica suspension and the resulting mixture was heated to approximately 95 °C and stirred for 65 h. To overcome the problem of losing water during a long time heating, water was topped up several times and the flask was covered with parafilm to reduce evaporation. Once the reflux was completed, urea was then added. The mixture was refluxed further for 55 h. The solution was then allowed to cool to room temperature and filtered to give the stevensite as a white gel. Powder X-ray diffraction (PXRD) pattern of a dried stevensite specimen shows several crystalline phases including calcium magnesium silicate hydroxide hydrate and magnesium aluminium hydroxide carbonate hydrate. However, the major phase is non-crystalline (Figure S1, Supporting Information, SI).

In a typical synthetic procedure for calcite spherulites, 5.0 mmol calcium chloride was dissolved in deionised water (400 mL) to make solution A and 5.0 mmol sodium carbonate was also dissolved in deionised water (400 mL) to make solution B. 10 mg sodium alginate and/or 10 mg stevensite were added into 100 mL water under stirring to form a white suspension, to which was added solution A, followed by adding solution B. The mixed solution was made up to 1 L with further addition of deionised water. The final solution was then left for the crystals to grow. More than 10 solid samples were collected after reaction time from 5 min to 168 h, dried at 70 °C, for further analysis.

Sample characterization. A piece of natural sample or a synthesized sample containing many spherulites was ground into powder with a mortar and pestle. The crystalline phases were detected by using PXRD on a PANalytical Empyrean diffractometer using copper K_α radiation with λ = 1.5418 Å. The results of PXRD were processed by using Highscore Plus software. Morphology of the particles were revealed by scanning electron microscopy (SEM) on either Jeol JSM-5600 microscope with a resolution of ca. 3 nm or Jeol JSM-6700F field emission gun microscope with a resolution ca. 1 nm. Bulk specimens for SEM were sputter coated with a thin Au film using a Quorum Technologies Q150R ES sputter coater/carbon coater, in order to prevent the sample from charging. Microstructures of the samples were determined using HRTEM, selected-area electron diffraction (SAED) on a Jeol JEM-2011 transmission electron microscope operating at an accelerating voltage of 200 kV. Specimens for TEM were prepared either by crushing bulk samples into fine powder or by cutting bulk sample into thin plates using focused ion beam (FIB) on a FEI Scios FIB/FEG-SEM dual-beam microscope. The ion beam worked by wetting a sharp tungsten needle with a Ga liquid metal ion source (LMIS). To detect local compositions and elemental distribution in the samples, energy dispersive X-ray spectroscopy (EDX) was performed on an Oxford INCA system, which was equipped in the JSM-5600 microscope.

3. RESULTS AND DISCUSSION

3.1 Naturally occurring spherulites

Initial characterization of the spherulite-containing rock samples was carried out on PXRD (Figure S2 in the SI). The main crystalline phase is calcite, which has a rhombohedral structure with the unit cell parameters, a = 4.9890 Å and c = 17.0620 Å (PDF No. 00-005-0586). Some minor phases, such as silica, magnesium aluminium silicate hydroxide, are also detected. From the investigation of the local composition as described later, we found calcite is mainly in spherulites and other crystalline phases are in the surroundings. It has been commonly accepted that calcite is the most thermodynamically stable phase of $CaCO_3$.[20]

From SEM images of the bulk sample, we can see many spherulites exposing to the surface (Figure S3a in the SI). The rock specimen was then pretreated with two approaches. In the first, the samples were washed in a 0.5% HCl solution for approximately 60 seconds as an acid-etching pretreatment. The acid helped to broaden the gaps between the crystalline particles within the rock sample. This treatment might cause a slight damage to the microstructure, but it made it much easier to distinguish the spherulites and their surroundings (Figure 2a). Another method was grinding and polishing using different types of abrasive paper; 240 grits and 600 grits, as well as a 3 μm polishing mop. This flattened the surface of the sample and made it easier to view the cross section by SEM. It also caused less damage of the sample as the original structure remained the same. However, it could be difficult to identify some specific structures (Figure 2b).

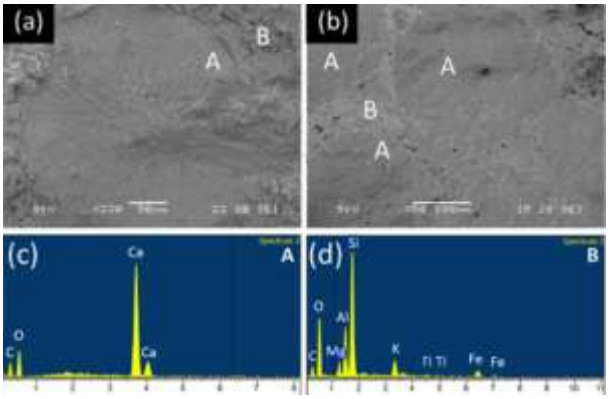

Figure 2. SEM images of rock samples treated (a) by acid-etching and (b) by grinding and polishing. A: spherulites; B: surroundings. EDX spectra obtained from (c) an area of A and (d) an area of B of the sample in (a).

Using both methods, spherulites (A) and surroundings (B) of the rock sample are identified in the SEM images. The latter seems to be porous, similar to the previously observed porous surrounding materials of the magnesium-clay minerals in lacustrine carbonate reservoirs in the Pre-Salt Barra Velha Formation off the coast of Brazil.[21] EDX point analysis on spherulites marked 'A' in Figure 2a, showed only C, O and Ca elements, indicating possible $CaCO_3$ (Figure 2c). From the surrounding materials, marked 'B', on the other hand, Ca was not detected by EDX, while many other elements were present, such as Si, Al, Mg, K, Fe, Ti, O, C, etc (Figure 2d). There is no discernable compositional difference in the acid-treated and polished samples.

EDX elemental mapping has also been performed to examine the distributions of all elements in a selected area of a rock specimen containing several spherulites as shown in Figure 3. The results are consistent with the EDX point analysis shown in Figure 2. However, elemental mapping offers some more detailed information of elemental distributions. Ca is mainly seen in the spherulites. But some very small particles and large layers may also be Ca rich. The carbon concentration is slightly higher in the surrounding substrate than in the spherulites. However, the highest concentration of carbon is at the surface of the spherulites, where oxygen content is low. It probably indicates that the spherulites are covered by a thin layer of C-rich substance, which could be the residue of decomposed organic compounds. More detailed investigation of this C-rich layer was carried out (Figure S4 in the SI). In some areas, this C-rich layer is very thick (Figure S5 in the SI). Apart from this layer associated with calcite particles, oxygen concentration in the whole area is almost uniform. Si, Fe and Al only present in the surroundings. It is surprising to find presence of Mg and K in the spherulites as well as in the surroundings. Since the spherulites consist of microrods, the space would be filled by organic compounds at least at an initial stage of the particle formation. Mg and K may exist with these organic compounds. On the other hand, Mg could substitute Ca in calcite.

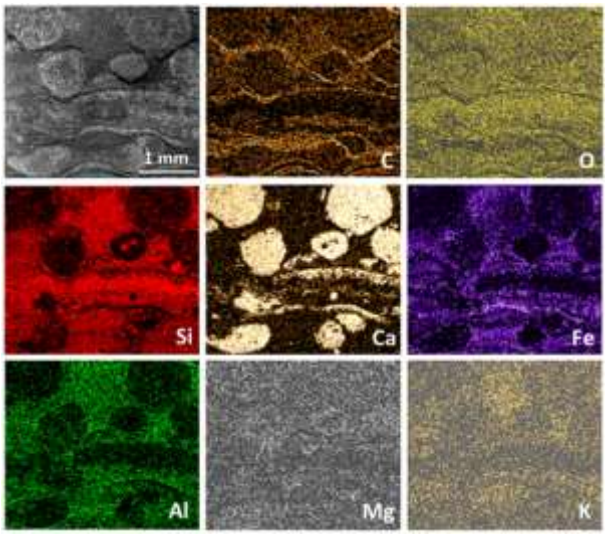

Figure 3. EDX elemental mapping of a piece of natural rock specimen containing some spherulites. Top left picture is the corresponding SEM image.

The microstructure of calcite spherulites can be described as a spherical core with deposition of multilayer radially orientated microrods, which can be revealed by an acid treatment (Figures S3b

in the SI, 4a). To further investigate the microstructure of spherulites, a focused ion beam cutting was conducted. Figure 4a is a high-resolution SEM image of a cross section of a natural spherulite. Multilayer radially arranged microrods, similar to the microstructure of the spherulites collected from a fresh limpet shell,[17] are also visible. The reason for the uniform length of the microrods in the same layer is still unknown. A linear deposition of Pt on the sample surface was made along the radial direction as shown in Figure 4a, in order to protect the underneath plate sample during the FIB operation. The parts of specimen on both sides of the protected area of the sample were removed by the ion beam layer by layer. The final plate sample (inset in Figure 4a) was further thinned and polished until the thickness was reduced to about 100 nm, which was suitable for HRTEM imaging. The original location of the sample was maintained as indicated by the arrows.

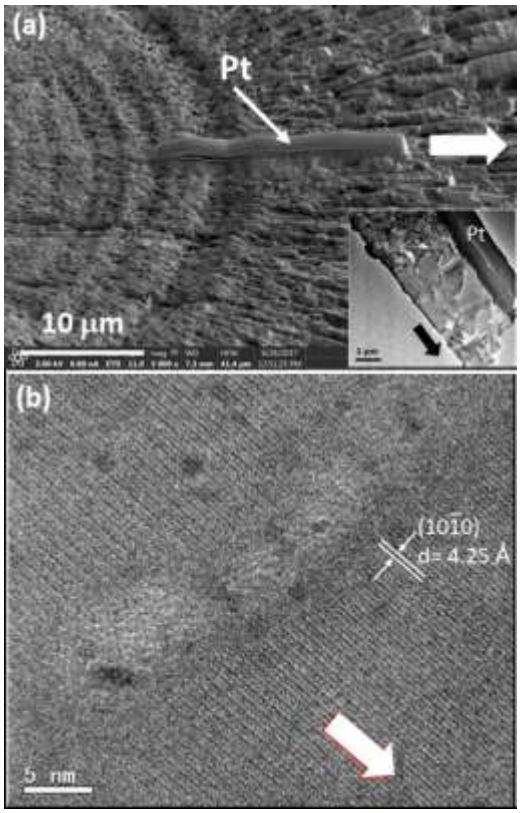

Figure 4. (a) High resolution SEM image of a cross section of a natural spherulite, showing multilayer microrods. Pt has been deposited for FIB preparation of a plate sample for HRTEM (inset). (b) HRTEM image from the specimen plate. The arrow indicates the [0001] direction, which is parallel to the radial direction as seen in (a).

Figure 4b shows a HRTEM image from the plate sample. It is confirmed that the longitudinal axis of the microrods lies along the radial directions of the spherulite and is parallel to the [0001] zone axis of calcite. Some large cavities are also present. One possible reason of forming such cavities is that the initial crystallinity of the microrods was low, e.g. containing nanocrystallites embedded in a soft substrate. When these nanocrystallites join together to form larger crystals, some cavities are inevitably left in between the crystals. Some HRTEM images from edge of microrods show many nanocrystallites embedded in an amorphous network (Figure S6 in the SI).

3.2 Synthetic spherulites

Synthesis of calcite crystals under different conditions has been tried, in order to find the optimized conditions for spherulites, and finally to establish the formation mechanism. The main products obtained in 9 different groups are shown in Table 1.

In Group 1, a simple mixture of 5.0 mmol $CaCl_2$ and Na_2CO_3 solutions led to a quick formation of rhombohedral crystals (Figure S7 in the SI). It is a typical classical crystal growth in a supersaturated solution. The crystal size increases with the reaction time. The rhombohedral morphology satisfies a minimum surface energy and its formation can be well elucidated by The Bravais-Friedel-Donnay-Harker (BFDH) law [22-24] and the Hartman-Perdok theory.[25]

In Group 2, $CaCl_2$ solution mixed with stevensite suspension first, followed by addition of Na_2CO_3. Rhombohedral crystals were produced, similar to Group 1 (Figure S8 in the SI), without any spherulites. The only difference is that the crystals in Group 2 tend to intergrow and cross each other, appearing as spherical clusters, about 10 μm in diameter. A possible reason for this is a development of several nuclei close to each other on the surface of stevensite gel. It indicates that, in a pure inorganic synthetic system, the chemicals in stevensite do not offer any help in the formation of spherulites.

When $CaCl_2$ solution mixed with alginate solution, followed by addition of Na_2CO_3, with the overall composition of chemicals of 5 mmol $CaCl_2$, 5 mmol Na_2CO_3, and 10 mg alginate, the products in Group 3 are both spherulites and bulk crystals (Figure 5a). The spherulites are covered by a soft substance, which is likely to be alginate gel. The EDX data showed that the bulk rhombohedral crystals were pure $CaCO_3$. In the spherulites, however, in addition to the main phase of $CaCO_3$, Na, Cl, and extra C and O were also detected, indicating that the spherulites are composite of calcite and alginate.

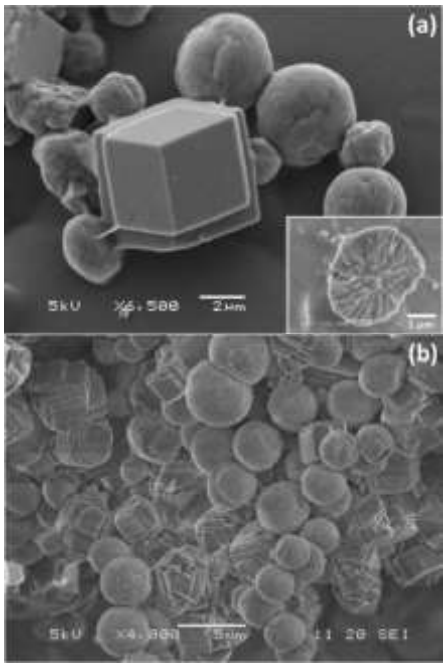

Figure 5. SEM images of the products of (a) Group 3, 0.5 h and (b) Group 5, 4 h, containing both spherulites and rhombohedral bulk crystals. The inset of (a) is a cross section SEM image of a spherulite with a reaction time (a) 5 min.

Sodium alginate, $(C_6H_7NaO_6)_n$, is water soluble. But in the presence of divalent cations, such as Ca^{2+}, Na^+ cations bound to the carboxylate groups are replaced by Ca^{2+} cations. Every two units of $(C_6H_7O_6)^-$ can house one Ca^{2+} cation. 10 mg sodium alginate as added in the Group 3 synthetic solution can only take 0.025 mmol Ca^{2+} at maximum, much lower than the actually added 5 mmol of Ca^{2+}. The excess Ca^{2+} cations left in the solution would inevitably react with CO_3^{2-} anions to form rhombohedral bulk crystals.

On the other hand, the Ca^{2+} cations bind to alginate, creating cross linkages to form a porous, insoluble gel network.[26] When Na_2CO_3 solution was added, CO_3^{2-} anions migrated into the calcium alginate gel, forming calcite nanocrystallites. The limited space and the difficulty of movement of charged ions inside the gel network inhibited further growth of these nanocrystallites. Instead, they aggregated to form spherulites. A cross section SEM image of a spherulite shown in the inset of Figure 5a demonstrates a radial arrangement of microrods. The principal driving force of the ordering of the nanocrystallites into such a novel microstructure is probably dipolar field as discussed in the previous reports on the formation of synthesized vaterite spherulites,[16] naturally occurring aragonite spherulites,[17] synthesized ZnO microspheres.[27,28]

It was noted that when the reaction time was increased to 24 h, the number of rhombohedral crystals significantly increased and the number of the spherulites decreased. The spherulites almost disappeared when the growth time was further increased to 48 h, leaving only rhombohedral crystals. This can be explained as follows. When all the Ca^{2+} in the calcium alginate gel contributed to the formation of calcite nanocrystallites, the released acidic sites in alginate would accept Na^+ cations and the polymer became soluble again. The calcite nanocrystallites would expose to the solution and dissolute, making contribution to the further growth of bulk crystals via Ostwald ripening.

In the synthesized samples in Group 4 with a mixture of 5 mmol $CaCl_2$, 5 mmol Na_2CO_3, 10 mg stevensite and 10 mg alginate, the product was very similar to that in Group 3 (Figure S9 in the SI), containing both calcite bulk crystals and spherulites. The stability of the spherulites was also poor. When the reaction time was increased to 48 h, no spherulite particles were observed. The rhombohedral crystals were the only product. Mixture of stevensite and alginate salts at this level did not offer a good protection for spherulites.

Since we found that alginate was essential in the formation of spherulites during our primary tests above, we increased the amount of added alginate. In Group 5, the additions of both stevensite and alginate were increased from 10 mg (Group 4) to 100 mg, in which most Ca^{2+} cations were still in the solution. Again, both spherulites and rhombohedral crystals in clusters were produced, as shown in Figure 5b.

The rhombohedral crystals exist as clusters of relatively smaller crystals. The spherulites seem to be denser than those in Group 3 (Figure 5a). More significantly, the spherulites in Group 5 specimens were much more stable. A composite gel of alginate and stevensite offers a better protecting network for the spherulites.

Further increasing alginate to 1000 mg without addition of stevensite, in Group 6, a high yield of spherulitic particles was achieved (Figure 6a). Since the added alginate has a capacity of housing only half of Ca^{2+} in the solution, rhombohedral crystals formed as well. Without the stevensite substrate, these rhombohedral crystals are small and separated without forming clusters. The spherulitic particles are large and not protected by an alginate coating layer. Consequently, the tips of microrods at their surface underwent further growth. The inset of Figure 6a shows an enlarged SEM image of an individual spherulite with less porous and higher crystallinity surface. The

arrows indicate small pieces of residue of alginate gel.

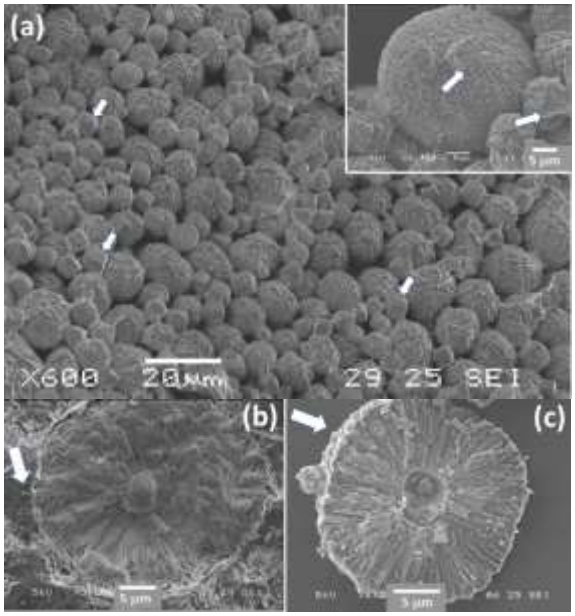

Figure 6. (a) SEM image of the product in Group 6 after reaction for 24 h. The arrows indicate small rhombohedral crystals. The inset shows an individual spherulite after reaction for 4 h with surface crystal expansion. The arrows indicate the residue of alginate. (b) A cross section SEM image of a spherulite after reaction for 1 week with a good protection by alginate (pointed by an arrow). (c) Another cross section SEM image of a spherulite after reaction of 24 h without alginate coating. The arrow points to a visible area with a surface crystal expansion.

Figure 6b is a cross section SEM image of a spherulite embedded in a soft network of alginate, showing the inner structure as well as the interface with its surrounding alginate gel. The needle like microrods radially arranged in the spherulite and a core particle are observed. No large crystals are visible at the interface. Figure 6c is a cross section image of another spherulite without alginate coating. Its surface has large crystalline tips, but the inner structure still contains fine microrods. The centre has a hole marking the location of a missing core, which might be similar to that seen in Figure 6b and was lost during the polishing process.

Figure 7 shows EDX point analysis of the core of a spherulite in comparison with the microrods. The latter is mainly $CaCO_3$ and the contents of C and O in the former are much higher. We then conclude that the core consists of randomly located calcite nanocrystallites as seen from the image contrast and a large proportion of alginate.

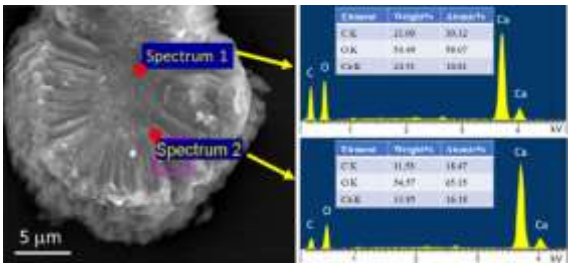

Figure 7. EDX spectra from the core and calcite microrods of a spherulite in Group 6 with a reaction time of 24 h.

It is interesting to see that the spherulites from Group 6 samples are very stable and no morphology transformation from spherulites to rhombohedral crystals took place in a long time, up to 2 weeks. The PXRD pattern from Group 6 sample with reaction time of 30 min shows only crystalline phase of calcite as shown in Figure S10 in the SI.

To avoid surface re-crystallization in the spherulites, 1000 mg of both alginate and stevensite were added in the system (Group 7, Table 1). Interestingly, all the spherulites are embedded in a thick gel network as shown in Figure 8. Therefore, surface re-crystallization would not occur. The uneven image contrast of the gel indicates that it is not pure alginate, but a mixture of alginate and stevensite. Consequently, although alginate offers a suitable substrate for growing spherulites, stevensite also plays an important role in increasing the hardness and stability of alginate gel to protect the spherulites. The overall structure in Figure 8 now is similar to the naturally occurring rock samples (see Figure 3). Both the gel and the spherulites are stable. Even after reaction for 6 days, the spherulites were still intact (Figure S11 in the SI).

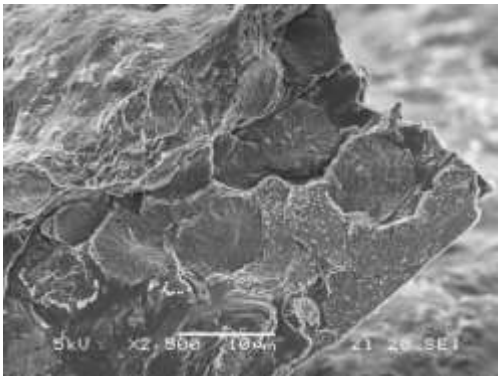

Figure 8. SEM image of a piece of specimen from Group 7 with 1000 mg alginate and 1000 mg stevensite, after reaction for 1 h.

In Group 8, 2000 mg alginate salt was added with absence of stevensite. The added ratio of $(C_6H_7NaO_6)^-$: Ca^{2+} was 2 : 1. Ideally, there were no excess Ca^{2+} left in the solution. The majority of particles are spherulites embedded in alginate gel. However, there are many spherical particles stay out of the gel. A small number of rhombohedral crystals were detected and the spherulites without alginate coating underwent surface re-crystallization (Figure S12 in the SI).

In Group 9, 2000 mg alginate and 2000 mg stevensite were used to create a stronger protection for spherulites. Indeed, most spherulites are embedded in the gel (Figure S13 in the SI). No rhombohedral crystals were observed.

3.3 Formation mechanism of calcite spherulites

To understand the building units of the spherulites and the whole formation mechanism, we collected specimens at very early stage of reaction and examined any crystalline particles. Figure 9a is a low magnification TEM image of a gel specimen in Group 6, being immediately collected when Na_2CO_3 solution was added in the synthetic system. Many calcite nanocrystallites evenly distribute in the gel. After reaction for 10 min., some spherical particles, about 10 μm in diameter, appeared as shown in Figure 9b.

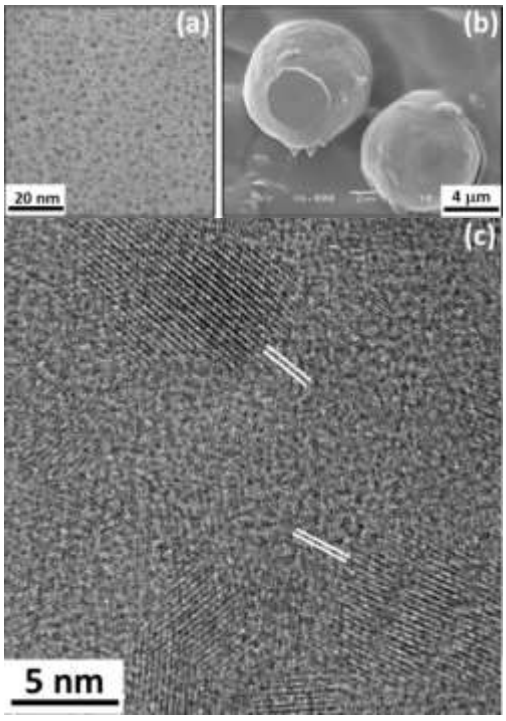

Figure 9. (a) TEM image of a gel formed immediately after mixing the precursor molecules in Group 6, showing a large amount of separated calcite nanocrystallites. (b) SEM image of two spherical gel particles after reaction for 10 min. (c) HRTEM image of a spherical gel showing randomly orientated calcite nanocrystallites. The marked fringes give a d-spacing of 2.84 Å, which can be indexed to (006) of calcite.

HRTEM images confirmed that these spheres were alginate gel containing high concentration of calcite nanocrystallites. Since the major component of the particles is organic, the samples were very sensitive to electron beam, and decomposed in seconds when normal beam brightness was applied. In our previous work, we found several ways of specimen treatment and careful control of microscopic conditions could significantly slow down the beam damage.[29] HRTEM images of many beam sensitive specimens were successfully obtained without any detectable damage, including C_{60}/trimethylbenzene composite nanowires,[30] MOF,[31] zeolites,[32,33] etc. In the present work, a gel sample was dehydrated, a thin edge of a disk was selected, a low dose of electrons was used, as many as possible microscopic conditions were pre-adjusted at a low magnification. HRTEM images of the gel sample were recorded (Figure 9c). The calcite nanocrystallites with lattice fringes and random orientation were clearly shown.

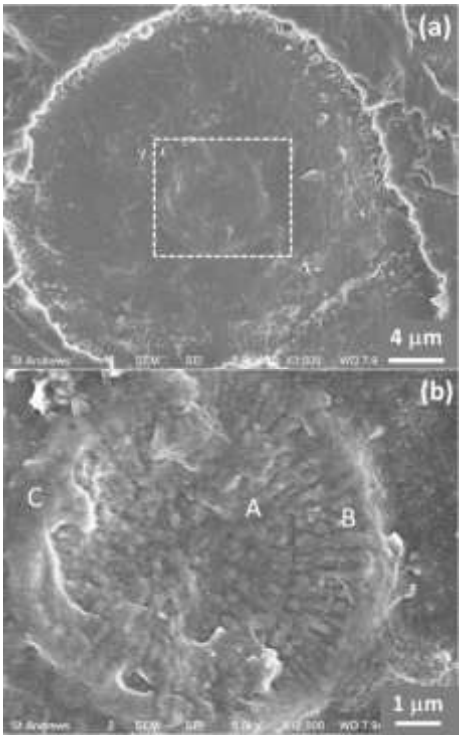

Figure 10. (a) Cross section SEM image of a spherulite from Group 6 after 2 h reaction. (b) An enlarged SEM image of the core as marked in (a), showing a disordered central area (A) and self-orientation of the nanocrystallites in the surface area (B). The outer surface of the core is covered by a thick alginate layer (C).

These nanocrystallites are believed to be the building units for spherulites. Figure 10 shows an early stage of aggregation of the nanocrystallites into short microrods with 300 nm wide and 1.5 μm in length on the surface of a spherical core of 5 μm in diameter. The microrods lie along the radial directions and are not yet developed into single crystals with some individual nanocrystallites being still recognised.

Based on the above results, we are able to propose the formation mechanism of the calcite spherulites. The crystals with such a novel morphology cannot form as free crystals in a solution. Alginate is essential. The detailed steps of the formation of spherulites are shown in Figure 11.

Step 1. Alginate has a log chain structure with multiple -COO- functional groups. When a sodium alginate solution mixes with a $CaCl_2$ solution, Ca^{2+} cations will substitute Na^+ and bind four -COO- groups by electrostatic interaction to form the so-called egg-box structure.[26,34] Calcium alginate is insoluble in water and, therefore, appears as a gel (Figure 11a).

Step 2. When Na_2CO_3 solution is added into the solution containing Ca-alginate gel, CO_3^{2-} anions will penetrate the gel to react with Ca^{2+} cations, forming calcite nanocrystallites (Figure 11b). The egg-box structure ensures an even distribution of Ca^{2+} cations, a large number of nucleation sites for calcite, and limit space for further crystal growth.

Step 3. When a high concentration of the nanocrystallites in the gel reaches locally, a spherical particle forms (Figure 11c). The calcite nanocrystallites seem to attract each other. It was proposed previously that nanoscale $CaCO_3$ crystals can have an interaction of dipolar field force.[16]

Step 4. The surface of the spherical particles is alginate-rich and negatively charged. These particles serve as the cores of the spherulites by further attracting the nanocrystallites, depositing on their surface in an ordered way to form microrods (Figure 11d). Again, dipolar field force works as the driving force for the radially arranged microrods.

Crystal structure of calcite can be regarded as a layered construction with alternative ionic layers of Ca^{2+} and CO_3^{2-} (Figure S14a in the SI). If the terminated surface of (0001) is a Ca^{2+} layer, the opposite layer ($000\bar{1}$) must terminate at CO_3^{2-}, in order to maintain the neutral state in the particle. When the particle size is large, the chance to have completely flat {0001} surface is small. A rough surface can self-cancel the charge (Figure S14b in the SI). On the other hand, even flat {0001} surfaces form in large crystals, the dipolar field strength is relatively weak because the force is proportionally to $1/r^2$. However, in nanocrystallites, the formation of flat surface is relatively easy and the inter-particle interaction based on dipolar field becomes significant (Figure S14c in the SI). Consequently, the $CaCO_3$ nanocrystallites can be charge-separated, which means individual nanocrystallites can be treated as small dipoles, assembling linearly on top of one another to produce the microrods in spherical particles.

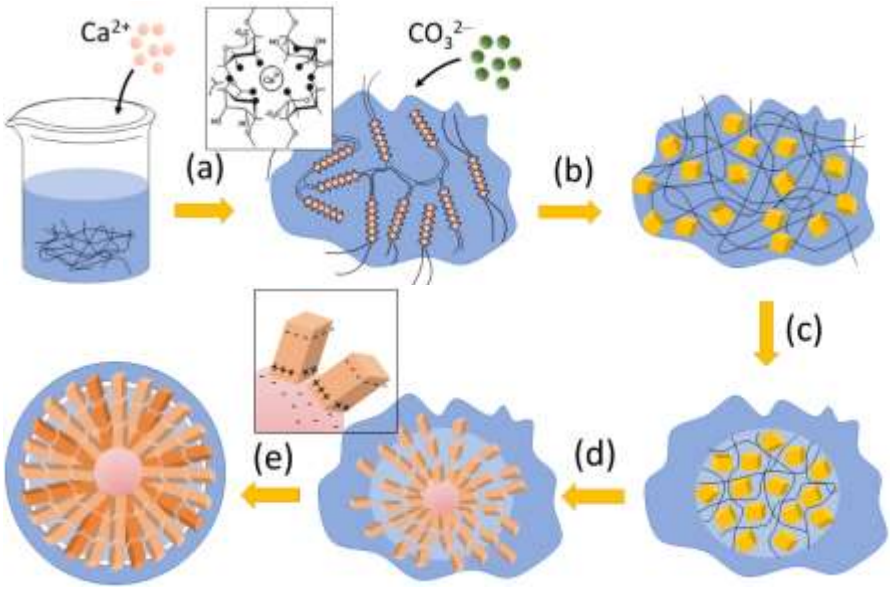

Figure 11. Schematic diagram representing the proposed formation mechanism of calcite spherulites embedded in a soft substrate of alginate and stevensite.

Step 5. The microrods further grow along the radial directions until all the separated calcite nanocrystallites in the alginate network are consumed. The spherulites grow up and their density increase. The inter-microrod space is filled by alginate gel and the surface of the spherulites is covered by alginate gel. It has been proved in the present work that inorganic stevensite does not directly promote the formation of the spherulites. However, by mixing with alginate, stevensite can adjust the hardness and improve the stability of the gel, and therefore, protect the spherulites.

CONCLUSIONS

The microstructure of naturally occurring spherulites and their surroundings collected from East Kirkton Quarry in Bathgate, Scotland has been investigated. Biomimetic synthesis of similar spherulites have been carried out and the formation mechanism has been proposed. The spherulites have a disordered organic/inorganic core and deposition of microrods on its surface in a radial arrangement. It is found that the formation of these spherulites is biotic and can only take place inside a biological soft substrate, followed by a protection of the soft substrate. In the present work, alginate has been used as a good example of the soft substrates. Inorganic silicates plays a role in hardening the gel, making a more stable protection for spherulites.

During the growth of spherulites, Ca^{2+} cations are captured by alginate first. CO_3^{2-} anions then penetrate into the alginate network, react with Ca^{2+}, forming calcite nanocrystallites. These nanocrystallites undergo self-assembly and self-orientation to form spherulites driven by dipolar field force. Since the nucleation sites and the growth of nanocrystallites are inside of the biological soft network, the previously proposed solution-based formation mechanisms are inappropriate. Abiotic process is not correct, because the co-occurring minerals do not directly promote the formation of the spherulites, although they may make a significant contribution to the protection of the spherulites. Our work supports a biotic process, in which alginate acts as extracellular polymeric substance to promote the growth of spherulites. The role of alginate in the reaction of $Ca^{2+} + CO_3^{2-} = CaCO_3$ is not a normal catalyst to reduce its activation energy in order to increase the reaction rate. Alginate's role is to increase the activation energy and reduce the reaction rate, leaving enough time for nanocrystallites to aggregate instead of growing into large bulk crystals.

ASSOCIATED CONTENT

Supporting Information

The Supporting Information is available free of charge on the ACS Publications website at DOI: Extra Figures are attached. Figure S1: PXRD of synthetic stevensite. Figures S2: PXRD; S3: SEM images; S4: EDX; S5: EDX elemental mapping; S6: TEM sample preparation by FIB and HRTEM image of rock sample containing calcite spherulites. SEM images of synthetic specimens in Group 1 (Figure S7), Group 2 (Figure S8), Group 4 (Figure S9), Group 7 (Figure S11), Group 8 (Figure S12), and Group 9 (Figure S13). Figure S10: PXRD of group 6. Figure S14: Schematic drawing of the calcite structure, and formation of dipolar field.

AUTHOR INFORMATION

Corresponding Author

*E-mail: wzhou@st-andrews.ac.uk
ORCID
Wuzong Zhou: 0000-0001-9752-7076

Notes

The authors declare no competing financial interest.

ACKNOWLEDGMENT

STW thanks China Scholarship Council and University of St Andrews for a CSC-St Andrews scholarship, and Ye Cheng for her helpful discussions on ancient materials. We also thank Michael Flowerdew for useful comments.

REFERENCES

(1) Verrecchia, E. P.; Freytet, P.; Verrecchia, K. E.; Jean-Louis Dumont, J.-L. Spherulites in calcite laminar crusts: biogenic $CaCO_3$ precipitation as a major contributor to crust formation. *J. Sediment. Res.* **1995**, *65*, 690–700.

(2) Buczynski, C.; Chafetz, H. S. Habit of bacterially induced precipitates of calcium carbonate: Examples from laboratory experiments and recent sediments. In *Carbonate Microfabrics*, Springer: **1993**, 105–116.

(3) Morse, H. W.; Donnay, J. D. H. Optics and structure of three-dimensional spherulites. *Am. Mineral.* **1936**, *21*, 391–426.

(4) Gardner, J. E.; Befus, K. S.; Watkins, J.; Hesse, M.; Miller, N. Compositional gradients surrounding spherulites in obsidian and their relationship to spherulite growth and lava cooling. *Bull. Volcanol.* **2012**, *74*, 1865–1879.

(5) Wright, V. P. Lacustrine carbonates in rift settings: The interaction of volcanic and microbial processes on carbonate deposition. *J. Geol. Soc. Lond. Spec. Pub.* **2012**, *370*, 39–47.

(6) Wright, V. P.; Barnett, A. J. An abiotic model for the development of textures in some South Atlantic early Cretaceous lacustrine carbonates. *J. Geological Soc., Lond., Spec. Pub.* **2015**, *418*, 209–219.

(7) Clarkson, E. N. K.; Milner, A. R.; Coates, M. I. Paleoecology of the visean of East Kirkton, West-Lothian, Scotland. *Earth Environ. Sci. Trans. R. Soc. Edi.* **1994**, *84*, 417–425.

(8) Mercedes-Martin, R.; Brasier, A. T.; Rogerson, M.; Reijmer, J. J. G.; Vonhof, H.; Pedley, M. A depositional model for spherulitic carbonates associated with alkaline, volcanic lakes. *Mar. Pet. Geol.* **2017**, *86*, 168-191.

(9) Zelenkova, M.; Sohnel, O.; Grases, F. Ultrafine structure of the hydroxyapatite amorphous phase in noninfectious phosphate renal calculi. *Urology* **2012**, *79*, 961–966.

(10) Granasy, L.; Pusztai, T.; Tegze, G.; Warren, J. A.; Douglas, J. F. Growth and form of spherulites. *Phys. Rev. E* **2005**. *72*, 011605.

(11) Banfield, J. F.; Welch, S. A.; Zhang, H.; Ebert, T. T.; Penn, R. L. Aggregation-based crystal growth and microstructure development in natural iron oxyhydroxide biomineralization products. *Science* **2000**, *289*, 751–754.

(12) Tosca, N. J.; Wright, V. P. Diagenetic pathways linked to labile Mg-clays in lacustrine carbonate reservoirs: A model for the origin of secondary porosity in the Cretaceous pre-salt Barra Velha Formation, offshore Brazil. *J. Geological Soc., Lond. Spec. Pub.* **2015**, *435*, 33–46.

(13) Rogerson, M.; Pedley, H. M.; Wadhawan, J. D.; Middleton, R. New insights into biological influence on the geochemistry of freshwater carbonate deposits. *Geochim. Cosmochim. Acta*. **2008**, *72*, 4976–4987.

(14) Kennedy, A. F.; Sutherland, I. W. Analysis of bacterial exopolysaccharides. *Biotechnol. Appl. Biochem*. **1987**, *9*, 12–19.

(15) Mercedes-Martin, R.; Rogerson, M. R.; Brasier, A. T.; Vonhof, H. B.; Prior, T. J.; Fellows, S. M.; Reijmer, J. J. G.; Billing, I.; Pedley, H. M. Growing spherulitic calcite grains in saline, hyperalkaline lakes: Experimental evaluation of the effects of Mg-clays and organic acids. *Sedimentary Geology* **2016**, *335*, 93–102.

(16) Greer, H. F.; Liu, M.-H.; Mou, C.-Y.; Zhou, W. Z. Dipole field driven morphology evolution in biomimetic vaterite. *CrystEngComm* **2016**, *18*, 1585–1599.

(17) Wu, S.; Chiang, C.-Y.; Zhou, W. Z. Formation mechanism of $CaCO_3$ spherulites in the myostracum layer of limpet shells. *Crystals* **2017**, *7*, 319.

(18) Doody, J. J.; McGill, R. A. R.; Darby, D.; Smythe, D. K. Geophysical surveys of the East Kirkton Limestone, Viséan, West Lothian, Scotland. *Trans. Roy. Soc. Edi.: Earth Sci*. **1994**, *84*, 197–202.

(19) Gombotz, W.; Wee, S. F. Protein release from alginate matrices. *Adv. Drug Delivery Rev*. **1998**, *31*, 267–285.

(20) Kawano, J.; Shimobayashi, N.; Miyake, A.; Kitamura, M. Precipitation diagram of calcium carbonate polymorphs: its construction and significance. *J. Phys.: Cond. Matter* **2009**, *21*, 425102.

(21) Terra, G. J. S.; Spadini, A. R.; França, A. B.; Sombra, C. L.; Zambonato, E. E.; Juschaks, L. C. da S.; Arienti, L. M.; Erthal, M. M.; Blauth, M.; Franco, M. P.; Matsuda, N. S.; da Silva, N. G. C.; Junior, P. A. M.; D'Avila, R. S. F.; de Souza, R. S.; Tonietto, S. N.; dos Anjos, S. M. C.; Campinho, V. S.; Winter, W. R. Carbonate rock classification for Brazilian sedimentary basins. *Boletim de Geociencias da Petrobras* **2010**, *18*, 9–29.

(22) Bravais, A. *Études Crystallographic*. Paris: Gauthier-Villars, **1866**.

(23) Friedel, M. G. Études sur la loi de Bravais. *Bull. Soc. Fr. Mineral Cristallogr*. **1907**, *30*, 326–455.

(24) Donnay, J. H.; Harker, D. A new law of crystal morphology extending the law of Bravais. *Am. Mineral*. **1937**, *22*, 446–467.

(25) Hartman, P.; Perdok, W. G. On the relations between structure and morphology of crystals, II. *Acta Crystallogr*. **1955**, *8*, 521–524.

(26) Morris, E. R.; Rees, D. A.; Thom, D.; Boyd, J. Chiroptical and stoichiometric evidence of a specific, primary dimerisation process in alginate gelation. *Carbohydr. Res*. **1978**, *66*, 145–154.

(27) Greer, H. F.; Zhou, W. Z.; Zhang, G.; Ménard, H. Nanocone decorated ZnO microspheres exposing the (0001) plane and enhanced photocatalytic properties. *Adv. Mater. Interfaces* **2017**, *4*, No. 1601238.

(28) Connolly, B. M.; Greer, H. F.; Zhou, W. Z. Formation mechanisms of ZnO spherulites and deritives, *Cryst. Growth Des.* **2019**, *19*, 249–257.

(29) Greer, H. F.; Zhou, W. Z. Electron diffraction and HRTEM imaging of beam sensitive materials. *Crystallogr. Rev*. **2011**, *17*, 163–185.

(30) Geng, J. F.; Zhou, W. Z.; Skelton, P.; Yue, W. B.; Kinloch, I. A.; Windle, A. H.; Johnson, B. F. G. Crystal structure and growth mechanism of unusually long fullerene (C60) nanowires. *J. Am. Chem. Soc*. **2008**, *130*, 2527–2534.

(31) Xiao, B.; Byrne, P. J.; Wheatley, P. S.; Wragg, D. S.; Zhao, X. B.; Fletcher, A. J.; Thomas, M.; Peters, L.; Evans, J. S. O.; Warren, J. E.; Zhou, W. Z.; Morris, R. E. Chemically blockable transformation and ultra-selective low pressure gas adsorption in a non-porous metal organic framework. *Nat. Chem*. **2009**, *1*, 289–294.

(32) Greer, H.; Wheatley, P. S.; Ashbrook, S. E.; Morris, R. E.; Zhou, W. Z. Early stage reversed crystal growth of zeolite A and its phase transformation to sodalite. *J. Am. Chem. Soc*. **2009**, *131*, 17986–17992.

(33) Wright, P. A.; Zhou, W. Z.; Perez-Pariente, J.; Arranz, M. Direct observation of growth defects in zeolite beta. *J. Am. Chem. Soc*. **2005**, *127*, 494–495.

(34) Grant, G. T.; Morris, E. R.; Rees, D. A.; Smith, P. J.; Thom, D. Biological interactions between polysaccharides and divalent cations: the egg-box model. *FEBS lett.* **1973**, *32*, 195–198.

For Table of Contents Use Only

Naturally Occurring and Biomimetic Synthesized Calcite Spherulites

Shitao Wu, Justine I. Blake, Li Guo and Wuzong Zhou

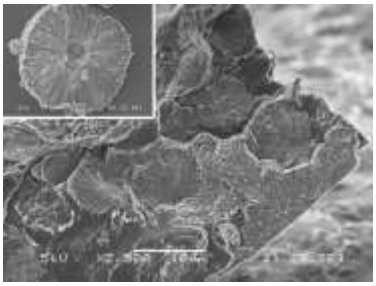

The microstructure of naturally occurring calcite spherulites collected from East Kirkton Quarry in Bathgate, Scotland has been investigated using XRD, EDX, SEM and HRTEM. Biomimetic synthesis of similar spherulites is performed using a mixture of alginate and stevensite as a structure directing agent. The formation mechanism of spherulites is proposed based on self-assembly and self-orientation of calcite nanocrystallites.